Isomer-tagged differential-plunger measurements in $^{113}_{54}$Xe

M. G. Procter,[1] D. M. Cullen,[1] M. J. Taylor,[1] J. Pakarinen,[2] K. Auranen,[2] T. Bäck,[2] T. Braunroth,[3] B. Cederwall,[2] A. Dewald,[3] T. Grahn,[2] P. T. Greenlees,[2] U. Jakobsson,[2] R. Julin,[2] S. Juutinen,[2] A. Herzáň,[2] J. Konki,[2] M. Leino,[2] R. Liotta,[2] J. Partanen,[4] P. Peura,[4] P. Rahkila,[4] P. Ruotsalainen,[4] M. Sandelius,[4] J. Sarén,[4] C. Scholey,[4] J. Sorri,[4] S. Stolze,[4] J. Uusitalo,[4] and C. Qi[2]

[1]*Schuster Laboratory, University of Manchester, Manchester M13 9PL, United Kingdom*

[2]*Department of Physics, Royal Institute of Technology, SE-10691 Stockholm, Sweden*

[3]*Institut für Kernphysik, Universität zu Köln, D-50937 Köln, Germany*

[4]*Department of Physics, University of Jyväskylä, FIN-40014 Jyväskylä, Finland*

(Received 13 October 2012; published 9 January 2013)

The 278-keV $M2$ γ decay from the $\nu h_{11/2}$ isomeric state in ^{113}Xe has been observed for the first time using the recoil-isomer tagging technique. The half-life of the isomer has been measured to be 6.9(3) μs. The derived $B(M2)$ value is in agreement with the trend of systematic measurements of $M2$ transition strengths in neutron-deficient tellurium and tin isotopes. The lifetime of the first excited state in the $\nu h_{11/2}$ band has been measured using the recoil distance Doppler-shift method. The extracted $B(E2)$ value has been compared to theoretical CD-Bonn calculations and recent lifetime measurements in ^{109}Te. This comparison of $B(E2)$ values has been used to shed light on the possible influence of collective degrees of freedom on $M2$ transition strengths in the most neutron-deficient xenon nuclei. The $\nu h_{11/2}$ band is deduced to have a degree of deformation comparable with the ground-state bands of the even-mass xenon isotopes. However, the value deduced in this work indicates a loss of collective behavior when compared with the lower-mass ^{109}Te. This result suggests that, while changes in deformation may be partly responsible for the observed trend in $B(M2)$ values for increasing Z, other effects may also be present.

DOI: 10.1103/PhysRevC.87.014308 PACS number(s): 21.10.Tg, 21.60.Cs, 23.20.−g, 27.60.+j

I. INTRODUCTION

Current research into the deformation of nuclei approaching the $N = Z = 50$ shell closure is providing new and intriguing results into the way protons and neutrons are observed to interact as the overlap of their wave functions becomes maximum [1–4]. The energies of the low-lying positive-parity states in nuclei that reside just outside of the $Z = 50$ shell closure are well reproduced from various models and the transition rates between these states have given valuable information with regards to evolving collectivity in this region of the nuclear chart ([4,5] and references therein). Previous studies of $M2$ decay rates in ^{111}Te and ^{115}Te have suggested that changes in $B(M2)$ values linking the low-lying positive-parity states with higher-lying negative parity sequences may be influenced by an increase in deformation compared with the near spherical $Z = 50$ tin nuclei [6]. Such $B(M2)$ values are well established in the odd-mass tin isotopes [7,8], and these show a clear trend with respect to neutron number about the midshell, where collective behavior is expected to be maximized.

Prior to the experiment discussed in this paper, no information was known on the $B(M2; 11/2^- \rightarrow 7/2^+)$ values in the neutron-deficient xenon isotopes [9–11]. The results presented in this paper give the first measurement of this decay strength in ^{113}Xe and point towards a smaller value in the neighboring nucleus ^{115}Xe. Owing to the lack of experimental measurements in other xenon isotopes, the lifetimes of states within the $\nu h_{11/2}$ band in ^{113}Xe have been compared with state-of-the-art shell-model calculations and our recent measurements in the lower-mass nucleus ^{109}Te [1]. The comparisons have aimed to assess the effects of changes in deformation on the measured $B(M2)$ strengths in these neutron-deficient nuclei.

II. EXPERIMENTAL METHODS AND DATA ANALYSIS

Excited states were populated in ^{113}Xe using the ^{58}Ni(^{58}Ni,2pn) reaction at a beam energy of 210 MeV. The K130 cyclotron, at the Accelerator Laboratory of the University of Jyväskylä, Finland, accelerated the ^{58}Ni beam onto a 1.05 mg cm^{-2} ^{58}Ni target foil. The target, as well as a 1.2 mg cm^{-2} Mg degrader foil, were mounted within the Differential Plunger for Unbound Nuclear States (DPUNS) [12] at the center of the JUROGAM-II γ-ray spectrometer [13]. DPUNS was operated within the helium-gas environment of the target chamber. This was possible owing to the use of a low-voltage, 45-V stepping motor and a low-voltage, 150-V piezoelectric attenuator, alleviating the need for carbon-isolating foils. The degrader foil acted to reduce the full velocity of the recoiling reaction products from $v/c = 0.038(1)$ to $v/c = 0.024(1)$. Prompt γ rays deexciting ^{113}Xe nuclei were collected in JUROGAM II comprising 15 Eurogam Phase-1-type single-crystal germanium detectors, located at backward angles of 158° and 134° to the beam axis and 24 clover detectors located in two detector rings either side of 90°. The recoil ion transport unit (RITU) [14] transported the fusion-evaporation residues to the GREAT focal plane spectrometer [15]. RITU was operated at a helium gas pressure of 0.9 mbar and separated from the vacuum of the beamline with the use of a roots differential pumping system. After passing through the multiwire proportional counter (MWPC) at the entrance to GREAT, nuclei were implanted at the focal plane into a pair of double-sided silicon-strip detectors (DSSDs). The separation of recoils and scattered beam was performed by imposing conditions on the time-of-flight signal, between the MWPC and the DSSD, and the energy loss within the MWPC. Isomeric and β-delayed γ-ray transitions were

subsequently observed in the GREAT planar germanium detector housed directly behind the DSSD. The planar strip detector had an absolute detection efficiency of ≈30% at 100 keV [15]. A recoil signal from the DSSD was used as a trigger for the creation of an event in the software and the energies of events occurring in all detectors were time stamped by a 100-MHz clock from the total data readout acquisition system [16].

Data were collected online using the GRAIN [17] software package and sorted into one-dimensional histograms and two-dimensional matrices to be analyzed offline with the RADWARE [18] and UPAK [19] software suites. Initially, for the analysis of the isomeric-delayed transitions, a matrix comprising delayed γ-ray energies versus the time between recoil implantation in the DSSD and γ-ray detection in the GREAT planar detector (E_γ-T matrix) was constructed. From this matrix, the half-life of the $\nu h_{11/2}$ isomer in ^{113}Xe was deduced (see Sec. III). Subsequent asymmetric matrices of prompt γ-ray transitions in each detector ring of JUROGAM-II versus correlated delayed γ rays (P-D matrix) were then constructed for each of the 26 different target-to-degrader distances used in this work. The prompt γ-ray transitions were correlated with both a recoil implantation in the DSSD as well as any γ ray detected in the GREAT planar detector within 20 μs ($3 \times T_{1/2}$) of an implantation. The matrices were also background subtracted in time using the interval 0–20 μs prior to a recoil implantation, removing γ-ray transitions associated with β-delayed decays or longer-lived isomeric states.

For the analysis of the recoil-distance Doppler-shifted lifetime data, recoil-isomer-tagged singles data were analyzed from the P-D matrices, corresponding to prompt γ-ray transitions observed in Ring 2 of the JUROGAM-II array. Located at a backward angle of 134° to the beamline, the ten detectors in Ring 2 afforded an appreciable Doppler shift while maintaining a significant number of statistics compared with the five detectors of Ring 1. The lifetime of the first excited state in the $\nu h_{11/2}$ band was determined using the differential decay curve method (DDCM) [20,21]. In the present work the lifetime of the level of interest, $\tau(x)$, was derived at each target-to-degrader distance, x using the relationship

$$\tau_i(x) = -\frac{Q_{ij}(x) - \alpha Q_{hi}(x)}{\mathrm{d}Q_{ij}(x)/\mathrm{d}t}\frac{1}{\langle v\rangle}, \qquad (1)$$

where Q_{ij} and Q_{hi} correspond to the normalized intensities of the fully Doppler shifted (s) components of the depopulating and feeding transitions, respectively. The intensities were normalized across each distance to the total number of recoil-gated prompt events observed at the target position. The term α is given by

$$\alpha = \frac{Q_{ij}(s) + Q_{ij}(d)}{Q_{hi}(s) + Q_{hi}(d)}, \qquad (2)$$

where $Q(s)$ and $Q(d)$ correspond to the normalized intensities of the fully Doppler-shifted and degraded components of the full photopeak, respectively, and accounts for the difference in intensities of the feeding and depopulating transitions. Finally, $\langle v\rangle$ is the mean velocity of the recoiling nuclei. The lifetime of the state under investigation was determined from a piecewise fit to the normalized fully Doppler-shifted components of the transition of interest. The derivative of this function, multiplied by the value of the lifetime, $\tau(x)$ was simultaneously fitted to the denominator in Eq. (1) and the χ^2 minimum was found. The weighted average of each individual lifetime value, within the so-called "region of sensitivity," was used to deduce the final lifetime value.

III. RESULTS

A previous study of ^{113}Xe managed to establish many of the low-lying positive-parity states, as well as the exact excitation-energy of the isomeric $\nu h_{11/2}$ level and a negative-parity band structure feeding it [9]. However, the half-life of the isomeric state and its decay path into the lower positive-parity states was not established. The half-life of the isomeric state was deduced from the E_γ-T matrix described in Sec. II. Exponential fits to the time spectra resulting from gates on two delayed transitions observed at 126- and 278-keV yeilded half-life measurements of 6.75(5) and 7.11(9) μs, respectively. The summed spectrum and combined fit, along with the mean half-life and standard deviation are given in Fig. 1(a).

Figures 1(a) and 1(b) show the results of gates set in the P-D γ-γ matrix constructed in this work using the measured half-life of the $\nu h_{11/2}$ state. The delayed spectrum resulting from a sum of gates on the most intense prompt transitions (415-, 657-, and 826-keV), assigned to ^{113}Xe in Ref. [9] is shown in Fig. 1(b). The previously established 126-keV transition linking the $7/2^+$ state to the $5/2^+$ ground state in ^{113}Xe, measured as 126.0(9) keV in this work, is clearly observed, along with Xe K_α and K_β x-ray peaks at 29.6(8) and 34.0(7) keV, respectively. Also present is a delayed γ-ray transition at 277.6(11) keV, consistent with the energy difference of 277 keV between the $7/2^+$ and $11/2^-$ states established in Ref. [9]. An analysis of a delayed planar-clover γ-γ matrix, while low in statistics, revealed these two transitions to be in temporal coincidence with each other, within a time window of 100 ns. Figure 1(c) shows the result of a sum of gates on the newly established delayed transitions in ^{113}Xe (126 and 278 keV). Many of the transitions established above the $\nu h_{11/2}$ state in the previous work are observed [9]. Figure 2 shows a partial level scheme for ^{113}Xe constructed from the isomer-tagged data collected in this work.

Table I gives the relative intensities for both the prompt and delayed transitions observed in this work, normalized independently. The initial and final spins have been taken from Ref. [9]. Figure 3 shows representative spectra resulting from gates placed on the delayed 126- and 278-keV transitions in six of the P-D γ-γ matrices at different target-to-degrader distances. The matrix was only incremented with γ-ray events recorded in Ring 2 of the JUROGAM-II array to best observe the shifting of each photopeak. The positions of the fully Doppler-shifted and degraded components of the 415-keV transition, linking the $15/2^-$ and $11/2^-$ states are shown in each panel, (a)–(f) in Fig. 3. To determine a value for the half-life of the $15/2^-$ state it was necessary to incorporate the measured intensity, at each target-to-degrader distance, of the 657-keV feeding transition in the analysis. The lifetime of the $15/2^-$ state was determined under the assumption that any unobserved feeding states had the same time properties

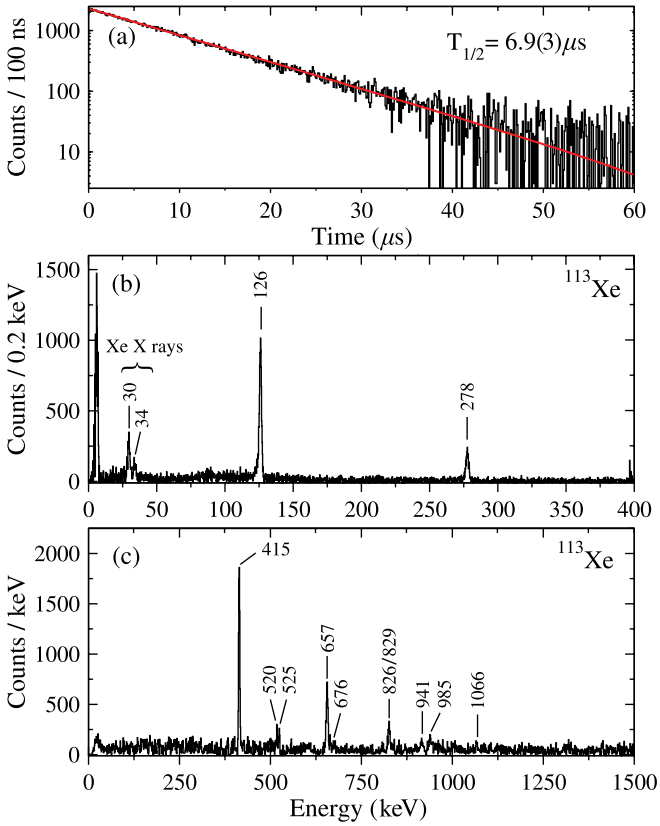

FIG. 1. (Color online) (a) A time spectrum for the 126- and 278-keV γ-ray transitions depopulating the $\nu h_{11/2}$ isomer. The time axis defines the time difference between a recoil implantation in the GREAT DSSD and a γ-ray detection in the GREAT planar detector. An exponential fit to the time spectrum is also shown. (b) A summation of spectra gated on the 415-, 657-, and 826-keV prompt transitions feeding the $\nu h_{11/2}$ isomeric state. The spectrum was also gated by the region of time from 0 to 20 μs after a recoil implantation into he DSSD. A background subtraction of 0–20 μs prior to implantation was also performed. (c) Summed spectrum of prompt γ-ray transitions resulting from gates placed on the delayed 126- and 278-keV transitions in ^{113}Xe with the same time conditions as (b).

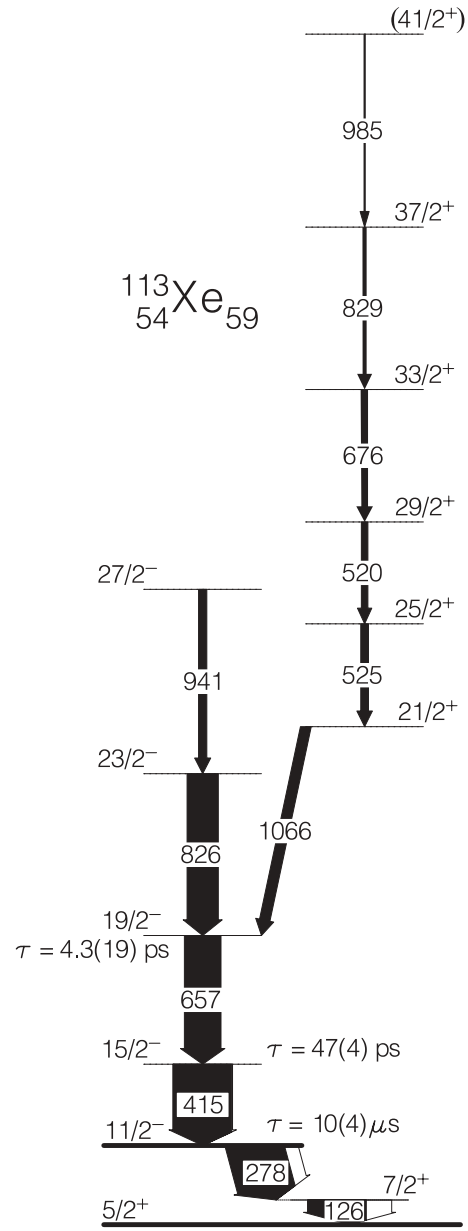

FIG. 2. Partial level scheme of states above and below the $\nu h_{11/2}$ isomer in ^{113}Xe identified from recoil-isomer tagging in this work. The widths of the arrows are proportional to the intensity of the transition, with the white component of each arrow indicating the calculated internal conversion component. Prompt and delayed transitions have been normalized independently. The energies and relative intensities of the 826- and 829-keV transitions are taken from Ref. [9].

as the measured feeding transition. This assumption has been successfully applied in previous lifetime measurements and is shown to be reasonable when both coincidence and singles data have been analyzed [22,23]. The unobserved feeding was accounted for in the α term from Eq. (1) which was deduced from a weighted average of the intensity branching ratio between the 415- and 657-keV transitions at each target-to-degrader distance. The branching ratio was corrected for efficiency as well as the effects of the angular distribution of each γ ray resulting from the use of solely backward angle detectors. Theoretical angular distributions were calculated for each transition assuming a mixing ratio of $\delta = 0$ and a typical substate population distribution of $\sigma = 3$, revealing an effect of <5% on the measured intensities. A systematic error of 5% was added to the statistical uncertainties in the peak fitting procedure to account for this.

The lifetime was deduced using the DDCM, as outlined in Sec. II, in the recoil-isomer tagged γ-ray singles mode. Figure 4 shows the fitting procedure for the analysis of the $15/2^-$ lifetime in ^{113}Xe performed in this work. The normalized intensities, Q_{ij} of the shifted component of the 415-keV transition are shown in the middle panel along with a three second-order polynomial piecewise fit. The derivative of the fit [denominator in Eq. (1)], shown in the bottom panel, has been simultaneously fitted to the difference in intensities of the 415- and 657-keV transitions [numerator in Eq. (1)] multiplied by the derived lifetime, τ, and corrected for the branching ratio between the two transitions, α. The value of

TABLE I. Intensities and γ-ray energies for ^{113}Xe measured in this work. The prompt and delayed intensities have been normalized separately. The initial and final spins are based upon those reported in Ref. [9]

E_γ (keV)	I_γ	$J_i^\pi \rightarrow J_f^\pi$
	Delayed decays	
29.6(8)	45(3)	K_α x ray
34.0(7)	12(2)	K_β x ray
126.0(9)	100(5)	$7/2^+ \rightarrow 5/2^+$
277.6(11)	98(7)	$11/2^- \rightarrow 7/2^+$
	Prompt γ rays	
414.6(2)	100(3)	$15/2^- \rightarrow 11/2^-$
519.7(8)	11(2)	$29/2^+ \rightarrow 25/2^+$
525.1(7)	13(2)	$25/2^+ \rightarrow 21/2^+$
656.7(3)	62(2)	$19/2^- \rightarrow 15/2^-$
676.2(3)	8(1)	$33/2^+ \rightarrow 29/2^+$
827.3(7)[a]	62(6)[a]	$23/2^- \rightarrow 19/2^-$
827.3(7)[a]	62(6)[a]	$37/2^+ \rightarrow 33/2^+$
940.6(4)	14(3)	$27/2^- \rightarrow 23/2^-$
984.6(11)	2(2)	$(41/2^+) \rightarrow 37/2^+$
1066.4(8)	18(3)	$21/2^+ \rightarrow 19/2^-$

[a]Combined energy and intensity of the 826- and 829-keV doublet transitions.

$\tau(x)$, shown in the top panel, was determined at each distance from a χ^2 minimization of the fits and a weighted average of points that lie within the region of sensitivity. The lifetime of the $19/2^-$ state was simply derived from an exponential fit to the normalized fully Doppler-shifted intensities of the 657-keV transition under the assumption that any feeding transitions had the same deformation as the state under investigation. The lifetime of the $19/2^-$ state was found to be 4.3(19) ps.

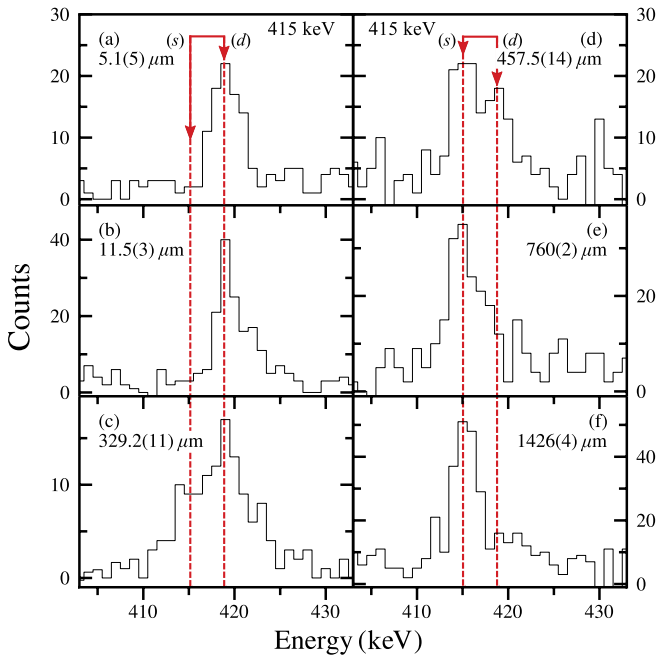

FIG. 3. (Color online) Recoil-isomer-tagged prompt spectra of the $15/2^- \rightarrow 11/2^-$ transition in ^{113}Xe. Each panel shows data collected at a different target-to-degrader separation. A Doppler-shift correction of $v/c = 0.0395$ has been applied to the data.

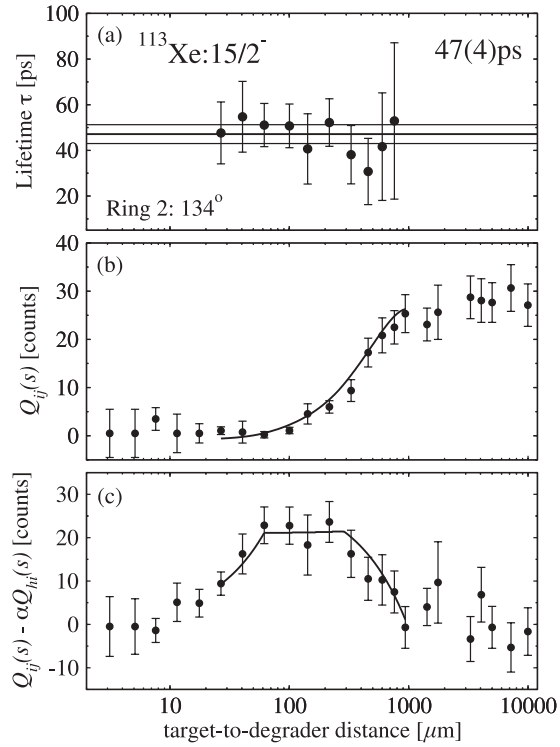

FIG. 4. Lifetime analysis of the $15/2^-$ state in ^{113}Xe. Panel (b) shows the efficiency corrected intensities of the fully Doppler-shifted components of the 415-keV transition measured in detector Ring 2. The curve has been fitted piecewise with three second-order polynomials. Panel (c) shows the difference in intensity of the shifted components of the 415-keV transition and the 657-keV transition feeding the $15/2^-$ state multiplied by α. The curve corresponds to the derivative of the fitting function in the middle panel multiplied by the value of τ derived from the analysis. Panel (a) shows the lifetime values determined from each target-to-degrader distance within the "region of sensitivity." The weighted average of each value is also given.

IV. DISCUSSION

A. The $\nu h_{11/2}$ isomeric state

The energy of the $11/2^-$ bandhead state has previously been established at 277 keV above the excitation energy of the $7/2^+$ state [9]. The $\nu h_{11/2}$ bandhead state in ^{113}Xe has been established to result from the single neutron occupancy of the $3/2^-[541]$ Nilsson orbital [10,11]. An analogous $h_{11/2}$ state is observed in ^{115}Xe; however, for the heavier ^{117,119,121}Xe isotopes, it is the $7/2^-$ state that represents the bandhead, resulting from the $5/2^-[532]$ orbital [10]. To date, the $7/2^-$ state has yet to be observed in ^{113}Xe or ^{115}Xe. This may suggest that the $7/2^-$ state lies above the $11/2^-$ bandhead, as the $E2$ decay linking the two states would be the preferential mode of decay compared with the more hindered $M2$ transition to the $7/2^+$ state.

The work presented in this paper has managed to establish the γ-ray decay linking the $11/2^-$ and $7/2^+$ states in ^{113}Xe

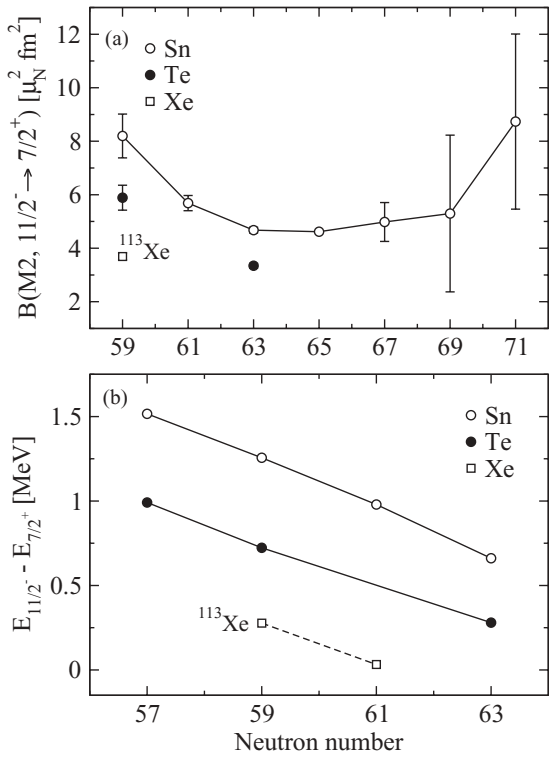

FIG. 5. (a) The systematics of the $B(M2; 11/2^- \rightarrow 7/2^-)$ in odd-A Te [6,25] and Sn [7,8] isotopes with the new measurement for ^{113}Xe. (b) The energy systematics of the $11/2^-$ state relative to the $7/2^+$ state in ^{109}Te [26,27], ^{111}Te [6], and ^{115}Te [25], and ^{107}Sn to ^{113}Sn [7,28]. The newly established decay in ^{113}Xe is included, as well as a point corresponding to the difference in energy between the $11/2^-$ and $7/2^+$ in ^{115}Xe, for which no decay has been observed to date.

for the first time. A comparison with the analogous decays in the lower mass neutron-deficient tellurium and tin isotopes suggests that the γ-ray transition depopulating the $\nu h_{11/2}$ state in ^{113}Xe would have an $M2$ multipolarity. An analysis of the intensities observed for the ^{113}Xe x-rays associated with the two delayed transitions corroborates this assumption. Assuming a pure $M1$ character for the 126-keV γ-ray transition linking the $7/2^+$ state and the $5/2^+$ ground state, the total calculated K shell internal conversion coefficient, α [24], for a 278-keV transition is expected to be 0.56, 0.94, and 3.25 for an $M2$, $E2$, and $E3$ multipolarity, respectively. Although outside of the uncertainties, the experimental value for α of 0.29(3) is in best agreement with the theoretical value for an $M2$ transition. The B(M2) value for a 278-keV γ decay, with a half-life of 6.93 μs, is calculated to be 3.69(13) μ_N^2 fm^2. Figure 5(a) shows the systematic $B(M2)$ values for the $11/2^- \rightarrow 7/2^+$ decays in odd-A Sn and Te isotopes, as well as the new measurement for ^{113}Xe determined in this work.

The experimental $B(M2)$ measurements in both the tin and the tellurium isotopes show a clear trend with neutron number. Particularly the neutron-deficient tin isotopes, where the $B(M2)$ strength is observed to decrease from $N = 59$ ^{109}Sn, reaching a minimum at ^{115}Sn, near the $N = 64$ subshell closure, finally increasing again to ^{121}Sn at $N = 71$. Figure 5(a) shows that the $M2$ transition strengths in both tin and tellurium nuclei are most hindered around the neutron midshell. Previous theoretical studies of the variation of $B(M2)$ values in the odd-mass neutron-deficient tin isotopes [7] explained the correlation with neutron number in terms of pairing effects and were able to achieve reasonable agreement with experimental values incorporating the effects of core polarization. The increase of ≈30% in the $M2$ hindrances of the measured tellurium isotopes has been attributed to the increase in deformation of the tellurium nuclei compared with the Sn isotopes. Core-quasiparticle calculations explained this assumption through the coupling of excited 2^+ and 4^+ core states to the $11/2^-$ and $7/2^+$ states, leading to a reduction in the calculated $M2$ matrix elements [6]. The $B(M2)$ value measured for ^{113}Xe in this work gives an increased hindrance of ≈50% compared with the tin isotopes. This extra hindrance may be seen to arise from the further increase in deformation of ^{113}Xe when compared with ^{111}Te. In fact, for $N > 58$ the even-mass xenon $B(E2; 2^+ \rightarrow 0^+)$ values are well known, and on average display 4 times the experimental values across the entire chain of even-mass neutron-deficient tin isotopes [4]. Figure 5(b) shows the energy systematics of the $11/2^- \rightarrow 7/2^+$ decays in the neutron-deficient tin and tellurium nuclei, as well as the new transition observed in this work. No $M2$ transition has been established to link the negative-party band in ^{115}Xe to the low-spin positive-parity states [10,11]; however, if a decay were to proceed between the $11/2^-$ and $7/2^+$ states it would be with a γ-ray energy of 32 keV. This is shown in Fig. 5(b) and is observed to fit with the systematics shown by the tin and tellurium isotopes. An estimate for the half-life of a decay from this state can be made assuming a single $M2$ γ-ray transition with a $B(M2)$ value of 1.18 μ_N^2 fm^2 based upon the change in the $B(M2)$ value between ^{109}Sn and ^{111}Sn. Taking into account the large internal conversion for a transition of 32 keV gives an estimate for the half-life of ≈5.9 ms. To better compare the $B(M2; 11/2^- \rightarrow 7/2^+)$ value in ^{113}Xe measured in this work with those in the neighboring nuclei, the deformation of the $\nu h_{11/2}$ band has been measured near the bandhead.

B. Lifetime of the $15/2^-$ state

Experimental $B(E2)$ values were derived from the lifetime measurements performed in this work using the relationship

$$B(E2; I \rightarrow I-2) = \frac{0.082}{\tau(1+\alpha_{\rm tot})E_\gamma^5}, \qquad (3)$$

where $B(E2)$ is in e^2 fm^4, τ is in picoseconds, and E_γ is in MeV. The total internal conversion coefficient, $\alpha_{\rm tot}$ was taken from Ref. [24]. To interpret the experimental reduced transition probabilities for ^{113}Xe in this work, shell-model calculations have been performed using the realistic charge-dependent one-boson-exchange nucleon-nucleon (CD-Bonn) potential [29]. The potential was renormalized using the perturbative G-matrix approach [30]. Calculations were made using a proton/neutron model space consisting of the $0g_{7/2}$, $1d_{5/2}$, $1d_{3/2}$, $2s_{1/2}$, and $0h_{11/2}$ orbitals. The corresponding single-particle energies of the neutron $g_{7/2}$ and $d_{5/2}$ orbitals were taken to be 0.0 and 0.172 MeV [31], respectively. The

TABLE II. Experimental and theoretical excitation energies, relative to the $\nu h_{11/2}$ state, and $B(E2)$ values for states within the $\nu h_{11/2}$ band in ^{113}Xe. The theoretical $B(E2)$ values have been calculated using standard proton and neutron effective charges of $e_\pi = 1.5$ and $e_\nu = 0.5$, respectively.

J_i^π	→	J_f^π	$E_{ex,i}$ (keV)		$B(E2)$ (e^2 fm^4)	
			Exp.	Theo.	Exp.	Theo.
$15/2^-$	→	$11/2^-$	415	297	1400 (125)	1286
$19/2^-$	→	$15/2^-$	1072	881	1550 (680)	1314
$23/2^-$	→	$19/2^-$	1898	1716	–	1337
$27/2^-$	→	$23/2^-$	2839	2794	–	1330

single-particle energies of the remaining states, as well as the $T = 1$ part of the monopole interaction, were determined using a global optimization method [32] by fitting to 157 low-lying yrast states in a range of $Z = 50$ tin nuclei between $102 \leqslant A \leqslant 132$. The optimized interaction has been observed to reproduce the experimental data within an average deviation of 130 keV. The $T = 0$ part of the monopole interaction is not optimized owing to computational limitation; the dimension around the midshell is currently too large to handle when both protons and neutrons are present. For the same reason, the calculations for ^{113}Xe were restricted to allow only one neutron excitation into to the $h_{11/2}$ orbital. The calculations assumed isospin symmetry and the proton single-particle energies were taken to be the same as those for the neutrons.

Table II compares the experimental and theoretical excitation energies and $B(E2)$ values for the transitions in the $\nu h_{11/2}$ band of ^{113}Xe.

The theoretical calculations are in good agreement with the experimental values, particularly the $B(E2)$ value measured in this work for the $15/2^- \rightarrow 11/2^-$ transition. This is in contrast to recent measurements of the analogous transition in ^{109}Te, where the same theoretical calculation was seen to underestimate the reduced transition strength by a factor of two [1]. Only with an increased neutron effective charge of $e_\nu = 0.8e$ was the theory able to achieve reasonable agreement with the experimental value. However, the near constancy of the $B(E2)$ values as a function of increasing spin within the band measured in this work was also observed in ^{109}Te, both experimentally and theoretically [1].

The lifetimes of the first excited states in the even-mass neutron-deficient xenon isotopes are well established for $N > 58$ [33–36]. The $B(E2)$ values derived from these measurements reveal a large increase in deformation compared with $B(E2)$ measurements in the ground-state sequences of both the neutron-deficient tellurium and tin isotopes, between 2 and 3 times larger. Figure 6(a) shows the excitation energy ratios of the first two excited states in the ground-state sequences of the most neutron-deficient even-mass Xe isotopes [5,37–41] and in the $\nu h_{11/2}$ bands of the odd-mass isotopes [11,42] (relative to the excitation energy of the bandhead).

This ratio is an indicator of the amount of collectivity present in a particular nuclear configuration and shows that for $N < 63$ the $\nu h_{11/2}$ bands may exhibit a larger degree of collective behavior than the analogous transitions in the ground-state sequences of the even-mass isotopes. This

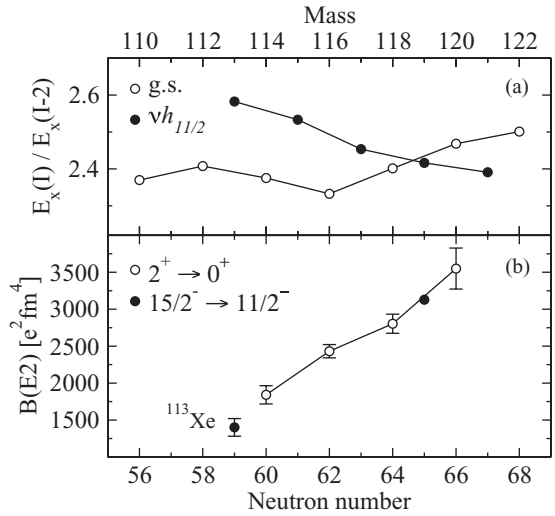

FIG. 6. (a) Excitation energy ratios of the first two excited states in the ground-state even-mass xenon isotopes [5,37–41] (white circles) and the $\nu h_{11/2}$ bands of the odd-mass isotopes (solid circles), relative to the $11/2^-$ state [11,42]. (b) $B(E2)$ values for the $2^+ \rightarrow 0^+$ decays in even-mass xenon isotopes [33–35] (white circles) and the $15/2^- \rightarrow 11/2^-$ decays in the odd-mass isotopes (solid circles). The $B(E2)$ value for ^{119}Xe is taken from a half-life measurement of ≈16 ps from Ref. [43].

behavior has been observed in ^{109}Te, where the equivalent $\nu h_{11/2}$ band was measured with a $B(E2)$ strength ∼2.5 times greater than the ground-state band of the neighboring ^{108}Te isotope [1].

Figure 6(b) shows the $B(E2; 15/2^- \rightarrow 11/2^-)$ value measured in this work along with the value for ^{119}Xe, $N = 65$, based upon a half-life measurement of ≈16 ps for the $15/2^-$ state [43], as well as the well established $B(E2; 2^+ \rightarrow 0^+)$ values in the most neutron-deficient even-mass xenon isotopes [33–35]. The $B(E2)$ value for ^{119}Xe appears to reproduce the trend observed in the excitation energy ratios, where the inferred deformation is predicted to be similar between the two bands around $A = 119$. However, the value measured in this work for ^{113}Xe ($N = 59$) may point towards a reduced $B(E2)$ value compared with the even-mass counterparts. Although this observation does not immediately conflict with the interpretation of the measured $B(M2)$ value for the decay of the $\nu h_{11/2}$ bandhead state, a comparison with the absolute $B(E2)$ value measured for the $15/2^-$ state in ^{109}Te [1] shows the measurement in this work to be smaller by almost a factor of 1.5. This observation may not support the argument that the observed trend in $B(M2)$ values for increasing proton number results from an increase in the deformation of the isomeric state. However, theoretical calculations in the previous work on ^{109}Te predicted a $B(E2)$ value smaller than both the measured and the theoretically calculated values in this work, in agreement with the postulate of an increasing deformation for the $\nu h_{11/2}$ band with increasing Z. Further measurements are required in the $\nu h_{11/2}$ bands of $^{115-117}$Xe, as well as theoretical calculations in both the odd and even-mass xenon isotopes, to fully address this issue.

V. CONCLUSIONS

In conclusion, recoil-isomer tagging has been used in conjunction with the JUROGAM-II-RITU-GREAT detector arrangement at the University of Jyväskylä to study the properties of the $M2$ decay from the isomeric $\nu h_{11/2}$ state in ^{113}Xe. The lifetime of the first excited state in the $\nu h_{11/2}$ band has been deduced from recoil-isomer tagged RDDS data collected with the DPUNS located at the the target position of JUROGAM II. The $B(M2; 11/2^- \rightarrow 7/2^+)$ value determined in this work follows the systematic trend observed from measurements of the analogous decays in the odd-mass tellurium and tin isotopes. To assess the effects of increasing deformation on the behavior of the $B(M2)$ values as a function of increasing Z the measured $B(E2)$ value in the $\nu h_{11/2}$ band has been compared with state-of-the-art shell-model calculations as well as recent measurements in the same band in ^{109}Te. While the value measured in this work points to a reduction in the deformation of the $\nu h_{11/2}$ band compared with the ground states of the even-mass xenon neighbors, the value is indicative of a significant amount of collective nuclear behavior. $B(E2)$ measurements in ^{109}Te, however, are observed to exceed those measured in this work by a factor of $\approx$1.5, suggesting that other factors currently unaccounted for may also be responsible for the trend in $B(M2)$ values as a function of increasing Z.

ACKNOWLEDGMENTS

M. G. Procter would like to thank Dr. A. Robinson for his assistance with the offline sorting of the raw data. This work has been supported by the EU 6th Framework Programme, "Integrating Infrastructure Initiative Transnational Access," Contract No. 506065 (EURONS), and by the Academy of Finland under the Finnish Centre of Excellence Programme 2006–2011 (Nuclear and Accelerator Based Physics Programme at JYFL). The authors acknowledge the support of GAMMAPOOL for the loan of the JUROGAM detectors. DPUNS was designed and built as a part of a collaboration between JYFL and The University of Manchester under the STFC Contract No. ST/G008787/1. T.B., B.C., R.L., and C.Q. acknowledge the support of the Swedish Research Council under Grants No. 621-2010-3694 and No. 621-2010-4723 and the Nordic Infrastructure support under NordForsk (Project No. 070315).

[1] M. G. Procter *et al.*, Phys. Rev. C **86**, 034308 (2012).
[2] T. Bäck *et al.*, Phys. Rev. C **84**, 041306 (2011).
[3] M. G. Procter *et al.*, Phys. Lett. B **704**, 118 (2011).
[4] A. Jungclaus *et al.*, Phys. Lett. B **695**, 110 (2011).
[5] M. Sandzelius *et al.*, Phys. Rev. Lett. **99**, 022501 (2007).
[6] K. Starosta *et al.*, Phys. Rev. C **61**, 034308 (2000).
[7] A. Vdovin, C. Stoyanov, and W. Andrejtscheff, Nucl. Phys. A **440**, 437 (1985).
[8] M. Fukuda, Y. Nagai, T. Irie, and H. Ejiri, Nucl. Phys. A **470**, 1 (1987).
[9] H. C. Scraggs *et al.*, Phys. Rev. C **61**, 064316 (2000).
[10] E. S. Paul *et al.*, Phys. Rev. C **53**, 2520 (1996).
[11] E. S. Paul, A. J. Boston, S. Courtin, P. J. Dagnall, J. L. Durell, C. Finck, B. Gall, B. Haas, F. Haas, F. Hannachi, F. Hoellinger, J. C. Lisle, A. Lopez-Martens, J. C. Merdinger, N. Rowley, H. C. Scraggs, O. Stezowski, B. J. Varley, and J. P. Vivien, Eur. Phys. J. A **7**, 449 (2000).
[12] M. J. Taylor *et al.*, AIP Conf. Proc. **1409**, 149 (2011).
[13] P. J. Nolan, F. A. Beck, and D. B. Fossan, Annu. Rev. Nucl. Part. Sci. **44**, 561 (1994).
[14] M. Leino *et al.*, Nucl. Instrum. Methods Phys. Res., Sect. B **99**, 653 (1995).
[15] R. D. Page *et al.*, Nucl. Instrum. Methods Phys. Res., Sect. B **204**, 634 (2003).
[16] I. Lazarus *et al.*, IEEE Trans. Nucl. Sci. **48**, 567 (2001).
[17] P. Rahkila, Nucl. Instrum. Methods Phys. Res., Sect. A **595**, 637 (2008).
[18] D. C. Radford, Nucl. Instrum. Methods Phys. Res., Sect. A **361**, 297 (1995).
[19] W. T. Milner (private communication).
[20] A. Dewald, S. Harissopulos, and P. von Brentano, Zeitschrift für Physik A Atomic Nuclei **334**, 163 (1989).
[21] A. Dewald, O. Möller, and P. Petkov, Prog. Part. Nucl. Phys. **67**, 786 (2012).
[22] P. Petkov *et al.*, Phys. Rev. C **62**, 014314 (2000).
[23] P. Petkov *et al.*, Nucl. Phys. A **543**, 589 (1992).
[24] T. Kibédi *et al.*, Nucl. Instrum. Methods Phys. Res., Sect. A **589**, 202 (2008).
[25] S. Vajda, A. Iordăchescu, E. Ivanov, and G. Pascovici, Phys. Lett. B **42**, 54 (1972).
[26] A. J. Boston *et al.*, Phys. Rev. C **61**, 064305 (2000).
[27] Z. Dombrádi *et al.*, Phys. Rev. C **51**, 2394 (1995).
[28] G. Auger, J. Lagrange, M. Pautrat, and J. Vanhorenbeeck, Nucl. Phys. A **426**, 109 (1984).
[29] R. Machleidt, Phys. Rev. C **63**, 024001 (2001).
[30] M. Hjorth-Jensen, T. T. S. Kuo, and E. Osnes, Phys. Rep. **261**, 125 (1995).
[31] I. G. Darby *et al.*, Phys. Rev. Lett. **105**, 162502 (2010).
[32] C. Qi and Z. X. Xu, Phys. Rev. C **86**, 044323 (2012).
[33] J. DeGraaf, M. Cromaz, T. E. Drake, V. P. Janzen, D. C. Radford, and D. Ward, Phys. Rev. C **58**, 164 (1998).
[34] I. M. Govil *et al.*, Phys. Rev. C **66**, 064318 (2002).
[35] J. C. Walpe *et al.*, Phys. Rev. C **52**, 1792 (1995).
[36] I. M. Govil *et al.*, Phys. Rev. C **57**, 632 (1998).
[37] J. Smith *et al.*, Phys. Lett. B **523**, 13 (2001).
[38] E. Paul *et al.*, Nucl. Phys. A **673**, 31 (2000).
[39] J. M. Sears *et al.*, Phys. Rev. C **57**, 2991 (1998).
[40] K. Loewenich *et al.*, Nucl. Phys. A **460**, 361 (1986).
[41] M. Serris *et al.*, Z. Phys. A **358**, 37 (1997).
[42] P. Chowdhury, U. Garg, T. P. Sjoreen, and D. B. Fossan, Phys. Rev. C **23**, 733 (1981).
[43] A. Chaudhury *et al.*, Bull. Am. Phys. Soc. 30, No. 4, 742, DE9 (1985).